recovery from mtDNA depletion. The same phenomenon has recently been observed in a mouse cell line after 2′,3′-dideoxycytidine–induced depletion (*22*). Results consistent with those described above were obtained in an experiment that used 2′,3′-dideoxycytidine to induce mtDNA depletion in HeLa cells (fig. S7) and in an experiment with EtBr carried out on 143B.TK$^-$ cells (fig. S5B).

Our data argue against the D-loop origins being sites of fork arrest of a replication initiating downstream of the D-loop. On the contrary, our findings are consistent with an active role of the D-loop–originating chains in mtDNA replication. Therefore, it appears that human cells exhibit two modes of mtDNA replication, each associated with distinct D-loop replication origins. One of these modes—a "maintenance mode" involving the position-57 origin and regulated at the level of this origin—appears to predominate in the maintenance, under steady-state conditions, of the copy number of mtDNA. The other mode—associated with the multiple previously known D-loop origins and regulated at the origins and at the premature termination site at the 3′-end of the D-loop—plays a major role in the initial recovery of the normal mtDNA complement after a depletion. This "induced" mode is possibly also involved in accelerating mtDNA synthesis to satisfy developmental, physiological, or aging-related demands. A decrease in termination has been shown to be responsible for the increased replication rate of mtDNA in proliferating T lymphocytes (*23*).

Although we have not addressed directly the current controversy concerning the mechanism of mammalian mtDNA replication, the evidence presented above has emphasized the importance of the D-loop origins in initiating mtDNA replication, in this respect supporting the original D-loop model.

References and Notes

1. H. Kasamatsu, D. L. Robberson, J. Vinograd, *Proc. Natl. Acad. Sci. U.S.A.* **68**, 2252 (1971).
2. D. L. Robberson, H. Kasamatsu, J. Vinograd, *Proc. Natl. Acad. Sci. U.S.A.* **69**, 737 (1972).
3. D. A. Clayton, *Cell* **28**, 693 (1982).
4. I. J. Holt, H. E. Lorimer, H. T. Jacobs, *Cell* **100**, 515 (2000).
5. M. Y. Yang *et al.*, *Cell* **111**, 495 (2002).
6. M. Bowmaker *et al.*, *J. Biol. Chem.* **278**, 50961 (2003).
7. D. F. Bogenhagen, D. A. Clayton, *Trends Biochem. Sci.* **28**, 357 (2003).
8. I. J. Holt, H. T. Jacobs, *Trends Biochem. Sci.* **28**, 355 (2003).
9. D. F. Bogenhagen, D. A. Clayton, *Trends Biochem. Sci.* **28**, 404 (2003).
10. J. Zhang *et al.*, *Proc. Natl. Acad. Sci. U.S.A.* **100**, 1116 (2003).
11. See supporting data on *Science* Online.
12. M. P. King, G. Attardi, *Science* **246**, 500 (1989).
13. S. Anderson *et al.*, *Nature* **290**, 457 (1981).
14. S. Crews, D. Ojala, J. Posakony, J. Nishiguchi, G. Attardi, *Nature* **277**, 192 (1979).
15. D. D. Chang, D. A. Clayton, *Proc. Natl. Acad. Sci. U.S.A.* **82**, 351 (1985).
16. D. Kang, K. Miyako, Y. Kai, T. Irie, K. Takeshige, *J. Biol. Chem.* **272**, 15275 (1997).
17. D. F. Bogenhagen, D. A. Clayton, *J. Mol. Biol.* **119**, 49 (1978).
18. G. G. Brown, G. Gadaleta, G. Pepe, C. Saccone, E. Sbisà, *J. Mol. Biol.* **192**, 503 (1986).
19. T. Ohsato *et al.*, *Biochem. Biophys. Res. Commun.* **255**, 1 (1999).
20. A. Wiseman, G. Attardi, *Mol. Gen. Genet.* **167**, 51 (1978).
21. K. Laderman *et al.*, *J. Biol. Chem.* **271**, 15891 (1996).
22. T. A. Brown, D. A. Clayton, *Nucleic Acids Res.* **30**, 2004 (2002).
23. Y. Kai *et al.*, *Biochim. Biophys. Acta* **1446**, 126 (1999).
24. The size of the fragment produced by Fnu4H1 (797 nt) is different from that expected from the mtDNA sequence (*13*) because of an A263G polymorphism present in 143B.TK$^-$ cell mtDNA [see MITOMAP: A Human Mitochondrial Genome Database (www.mitomap.org)].

25. Supported by NIH grant GM11726 (G.A.). We thank J. Zhang for providing additional data, A. Chomyn for valuable discussions and comments on the manuscript, and M. Roldan-Ortiz and R. Zedan for expert technical assistance.

Supporting Online Material

www.sciencemag.org/cgi/content/full/306/5704/2098/DC1
Materials and Methods
SOM Text
Figs. S1 to S7
References

28 June 2004; accepted 21 October 2004
10.1126/science.1102077

Phosphorylation of Proteins by Inositol Pyrophosphates

Adolfo Saiardi,[1]*† Rashna Bhandari,[1]* Adam C. Resnick,[1] Adele M. Snowman,[1] Solomon H. Snyder[1,2,3]‡

The inositol pyrophosphates IP_7 and IP_8 contain highly energetic pyrophosphate bonds. Although implicated in various biologic functions, their molecular sites of action have not been clarified. Using radiolabeled IP_7, we detected phosphorylation of multiple eukaryotic proteins. We also observed phosphorylation of endogenous proteins by endogenous IP_7 in yeast. Phosphorylation by IP_7 is nonenzymatic and may represent a novel intracellular signaling mechanism.

Inositol phosphates serve diverse biologic functions, with the best characterized, inositol 1,4,5-trisphosphate (IP_3), mediating the release of intracellular calcium stores. In mammals, inositol pyrophosphates, such as diphosphoinositol pentakisphosphate (5PP-IP_5, or IP_7) and bis-diphosphoinositol tetrakisphosphate ($[PP]_2$-IP_4, or IP_8) (*1–3*), are formed by a family of three evolutionarily conserved inositol hexakisphosphate (IP_6) kinases (IP6Ks) (*4*, *5*). Functions of inositol pyrophosphates include regulation of endocytosis (*6*), chemotaxis (*7*), and apoptosis (*8*).

The standard free energy of hydrolysis of the pyrophosphate bond in IP_7 has been estimated theoretically for the nonphysiological isomer 1PP-IP_5 at 6.6 kcal/mol, higher than that of adenosine 5′-diphosphate (ADP) (6.4 kcal/mol) and lower than that of adenosine 5′-triphosphate (ATP) (7.3 kcal/mol) (*1*). Moreover, the high steric constraints and strong electrostatic repulsion of the vicinal pyrophosphates in the naturally occurring IP_8 isomers (4,5)$[PP]_2$-IP_4 and (5,6)$[PP]_2$-IP_4 suggest that IP_8 would have a standard free energy of hydrolysis much higher than that calculated for IP_7 (*9*). These characteristics suggest that inositol pyrophosphates might serve as phosphorylating agents (*10*).

To determine whether proteins are phosphorylated by IP_7, we used mammalian IP_6 kinase 1 (IP6K1) and $\gamma[^{32}P]$ATP to synthesize IP_7 that was labeled at the β position of the pyrophosphate moiety, $5\beta[^{32}P]IP_7$ (Fig. 1A; fig. S1). To ensure that any apparent phosphorylation does not simply reflect binding of IP_7 to proteins, we synthesized $[^{32}P]IP_7$ labeled at position 2, which is not a pyrophosphate, and $[^{32}P]IP_6$ labeled at position 2 as controls (Fig. 1A). We compared phosphorylation by $5\beta[^{32}P]IP_7$ and $\gamma[^{32}P]$ATP by using equivalent specific activities and molar concentrations of each agent. In both mouse brain and yeast (*Saccharomyces cerevisiae*) extracts, we observed phosphorylation of multiple proteins with $5\beta[^{32}P]IP_7$ but not with either control agent (Fig. 1B). Moreover, incubation of cell extracts with $[^{32}PO_4]_i$ orthophosphate, at the equivalent specific activity and molar concentration as those used for $5\beta[^{32}P]IP_7$, revealed no incorporation of radiolabeled inorganic phosphate into proteins, ruling out the possibility that the phosphorylation by $5\beta[^{32}P]IP_7$ is a reflection of free

[1]Department of Neuroscience, [2]Department of Pharmacology and Molecular Sciences, and [3]Department of Psychiatry and Behavioral Sciences, Johns Hopkins University, School of Medicine, 725 North Wolfe Street, Baltimore, MD 21205, USA.

*These authors contributed equally to this work.
†Present address: Medical Research Council (MRC) Laboratory for Molecular Cell Biology and Cell Biology Unit, University College London, Gower Street, London WC1E 6BT, UK.
‡To whom correspondence should be addressed. E-mail: ssnyder@bs.jhmi.edu

$[^{32}PO_4]_i$ liberated by IP_7 phosphatases present in the cell extracts (Fig. 1B). Under these experimental conditions, 5β[^{32}P]IP_7 phosphorylated as many proteins as γ[^{32}P]ATP, but most of the labeled proteins were distinct for the two phosphate donors. As endogenous ATP in lysates may dilute γ[^{32}P]ATP, the observed phosphorylation by ATP may be an underestimate.

Apparent phosphorylation by IP_7 may merely reflect phosphorylation by ATP formed by IP_7 phosphorylation of ADP. However, 1 mM unlabeled ATP or ADP failed to diminish the extent of phosphorylation of mouse brain proteins by 5β[^{32}P]IP_7 (Fig. 1C). Moreover, 5β[^{32}P]IP_7 phosphorylated purified proteins in preparations that lack ADP (see below).

To ascertain the range of proteins phosphorylated by IP_7 in various tissues and species, we examined extracts of *Escherichia coli*, mouse brain, mouse kidney, and *Drosophila melanogaster*. Phosphorylation by IP_7 appears selective for eukaryotic organisms, as no proteins were phosphorylated by 5β[^{32}P]IP_7 in bacterial extracts. In contrast, abundant proteins were phosphorylated in the fly and mouse extracts with a number of differences between kidney and brain extracts (Fig. 1D).

If labeling with 5β[^{32}P]IP_7 reflects protein phosphorylation, then such phosphorylated sites should be subject to dephosphorylation and enhanced by phosphatase inhibitors (Fig. 1E). The phosphatase inhibitor sodium fluoride increased protein phosphorylation by 5β[^{32}P]IP_7 as well as γ[^{32}P]ATP. Inhibition of IP_7 pyrophosphatases by sodium fluoride (*2*) might also contribute to the observed effect. The more specific phosphatase inhibitors, okadaic acid and tautomycin, also increased protein phosphorylation in the presence of 5β[^{32}P]IP_7, whereas sodium orthovanadate and β-glycerol phosphate had no detectable effects.

Phosphorylation by 5β[^{32}P]IP_7 requires magnesium as a cofactor. Thus, phosphorylation of mouse brain proteins by 5β[^{32}P]IP_7 occurred only in the presence of divalent cations, with magnesium being more effective than manganese (Fig. 1F). Calcium could partially substitute for magnesium. In contrast, phosphorylation by ATP is comparable with manganese and magnesium but almost absent with calcium.

To identify specific proteins phosphorylated by IP_7, we focused on the three most prominent phosphoproteins (at 60, 63, and 98 kD) in yeast extracts. Proteins were partially purified (fig. S2), and matrix-assisted laser desorption/ionization (MALDI) mass spectrometry identified the 60-kD protein as NSR1 [the open reading frame (ORF) YGR159c], a nucleolar protein involved in ribosome assembly and export (*11*, *12*). The 98-kD protein was identified as YGR130c, a protein of unknown function. Both NSR1 and YGR130c that were overexpressed in yeast were phosphorylated by 5β[^{32}P]IP_7 (Fig. 2A). Treatment of extracts with lambda phosphatase, which acts on phosphorylated Ser, Thr, and Tyr residues (Fig. 2B), decreased phosphorylation by 5β[^{32}P]IP_7.

To identify the sites of phosphorylation, we generated deletion mutants of NSR1 for analysis. Phosphorylation occurred predominantly at amino acids 51 to 166 (Fig. 2D), a region containing extensive stretches of Ser residues surrounded by acidic amino acids. A smaller but similar acidic Ser domain is present in YGR130c (fig. S2). The acidic Ser region is critical for phosphorylation, as NAB4 (also know as HRP1, ORF YOL123w), a nuclear polyadenylated RNA-binding protein (*13*) that has RNA-binding sequences similar to those of NSR1 but that lacks the acidic Ser domain, was not phosphorylated by 5β[^{32}P]IP_7 (Fig. 2C). A sequence homol-

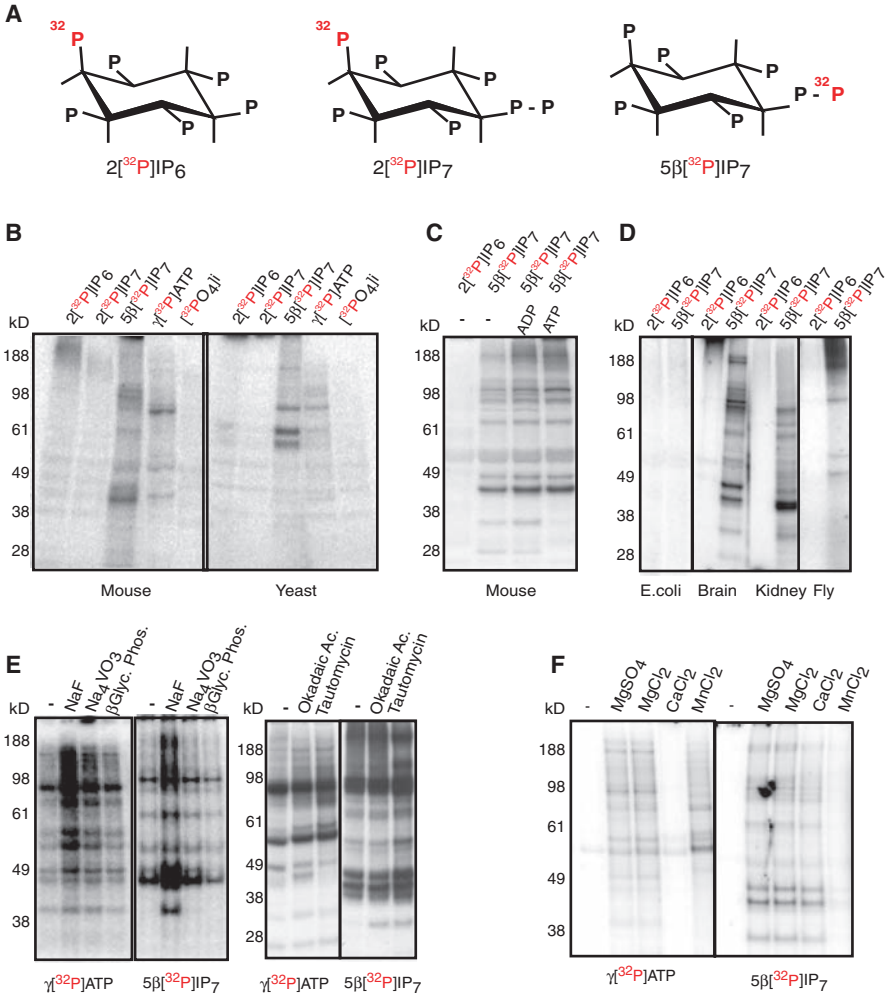

Fig. 1. Comparison of γ[^{32}P]ATP and 5β[^{32}P]IP_7 mediated protein phosphorylation. (**A**) Molecular structures of radiolabeled 2[^{32}P]IP_6, 2[^{32}P]IP_7, and 5β[^{32}P]IP_7. (**B**) IP_7 and ATP elicit phosphorylation in eukaryotic tissue. Crude extracts from mouse brain or yeast (20 μg), prepared without any protease or phosphatase inhibitors, were incubated with 0.1 μCi of 30 Ci/mmol 2[^{32}P]IP_6, 2[^{32}P]IP_7, 5β[^{32}P]IP_7, γ[^{32}P]ATP, or $[^{32}PO_4]_i$ for 1 hour at 37°C, followed by incubation in the presence of sample buffer at 95°C. Proteins were separated by polyacrylamide gel electrophoresis with NuPAGE (Novex), and the radiolabeled proteins were visualized by autoradiography. (**C**) Excess ADP or ATP fail to alter IP_7 phosphorylation. Mouse brain extract (*26*) was incubated with 0.5 μCi of 600 Ci/mmol radiolabeled inositols for 20 min at 37°C in the presence or absence of 1 mM unlabeled ATP or ADP. The samples were processed and visualized as above. (**D**) IP_7 phosphorylation in diverse species. Extracts from different organisms and tissues were incubated with labeled inositols as described in panel (C). (**E**) Protein phosphatase inhibitors augment IP_7 phosphorylation. Protein phosphorylation was performed as described in (C) in the presence or absence of the following protein phosphatase inhibitors: 0.5 mM NaF, 100 μM Na_3VO_4, 1 mM β-glycerol phosphate, 0.1 μM okadaic acid, and 0.1 μM tautomycin. (**F**) IP_7 phosphorylation requires divalent cations. Protein phosphorylation was performed as described in (C) by using 5 mM of the indicated bivalent cation as a cofactor.

ogy search of the yeast protein database revealed a substantial acidic Ser region in SRP40 (ORF YKR092c), a nucleolar protein that functions as a ribosomal chaperone (*14*). SRP40 overexpressed in yeast was also phosphorylated by 5β[^{32}P]IP_7 (Fig. 2C). SRP40 is the 63-kD target of 5β[^{32}P]IP_7 phosphorylation in yeast extracts on the basis of its loss of phosphorylation in extracts derived from SRP40-null (*srp40*Δ) yeast (Fig. 2E). Similarly, deletion of *nsr1* resulted in a loss of phosphorylation of the 60-kD protein. Because NSR1 and SRP40 are the principal proteins phosphorylated by 5β[^{32}P]IP_7, they could consume a major portion of endogenous IP_7. Hence, yeasts that do not have NSR1 or SRP40 (whose endogenous levels are only 15% those of NSR1) (*15*) might exhibit elevated levels of endogenous IP_7 and IP_8. IP_7 and IP_8 levels were doubled in mutant yeast lacking NSR1 compared with wild-type yeast but were unchanged in yeast lacking SRP40 (Fig. 2F). However, we cannot exclude that secondary consequences of *nsr1* deletion could indirectly alter IP_7 levels.

Although NSR1 consumes IP_7 within cells, it does not act as an IP_7 phosphatase (fig. S3). There was no detectable release of $[^{32}PO_4]_i$ orthophosphate in the presence of SRP40, YGR130c, or NSR1 under conditions in which these proteins were phosphorylated by 5β[^{32}P]IP_7. In contrast, the yeast IP_7 phosphatase, diphosphoinositol polyphosphate phosphohydrolase (DIPP, ORF YOR163w) (*16*), rapidly released $[^{32}PO_4]_i$ orthophosphate from 5β[^{32}P]IP_7 and did not undergo phosphorylation (fig. S3). These data rule out the possibility that apparent phosphorylation of proteins by IP_7 reflects a role for them as intermediates in a phosphohydrolase reaction.

To determine whether phosphorylation by IP_7 uses protein kinases, we examined phosphoproteins in the 89 viable null mutant yeast strains lacking each of the 122 known protein kinases (*17*). No striking alterations in the 5β[^{32}P]IP_7 protein phosphorylation pattern were observed in any of these mutants (*18*). In an in-gel kinase assay with purified NSR1, phosphorylation with 5β[^{32}P]IP_7 but not 2[^{32}P]IP_6 was observed, which ruled out the involvement of any protein kinase other than one that would have a molecular weight identical to NSR1 (Fig. 3A).

Heating increased the rate and extent of phosphorylation of substrates by 5β[^{32}P]IP_7, which further indicated that phosphorylation is nonenzymatic (Fig. 3B). There is no incorporation of [^{32}P]IP_7 labeled at position 2 nor of [^{32}P]IP_6 into purified SRP40 (Fig. 3C). Because the initial binding of IP_7 to the site of phosphorylation should require physiologic temperatures to ensure the appropriate conformation of the phosphorylation site, substantial phosphorylation of SRP40 by 5β[^{32}P]IP_7 was observed when conditions were first at 25°C followed by a 95°C treatment. No phosphorylation occurred if 5β[^{32}P]IP_7 was added after denaturing the proteins at 95°C or in presence of a chemical denaturing agent such as urea (Fig. 3D). Time-dependent phosphorylation of SRP40 and NSR1 at 37°C was also observed (Fig. 3E; fig. S4). Furthermore, 5β[^{32}P]IP_7-mediated phosphorylation of purified protein was detected in the presence of 50-fold excess of unlabeled IP_6, conditions that mimic the IP_6/IP_7 physiological ratio (fig. S4). Using multiple concentrations of unlabeled IP_7 (*18*), we determined that the K_m for IP_7-mediated protein phosphorylation was about 0.7 μM and the V_{max} was 0.1 μmol/mg per min. Although we detected 5β[^{32}P]IP_7-mediated phosphorylation of a fusion protein containing glutathione *S*-transferase and amino acid region 51 to 166 of NSR1 (Fig. 2D), no binding of [^{3}H]IP_6 or [^{3}H]IP_7 to this protein was detected (*18*). However, low affinity binding may have escaped detection.

To further characterize phosphorylation by IP_7, proteins phosphorylated by 5β[^{32}P]IP_7 were treated with acid or alkali. Phosphorylated YGR130c, SRP40, and NSR1 were more sensitive to alkali than to acid treatment (Fig. 3F), indicative of Ser/Thr phosphorylation (*19*). Furthermore, Western blot analysis of 5β[^{32}P]IP_7-phosphorylated SRP40 and NSR1 proteins with an antibody against phosphoThr revealed no phosphorylation on Thr (*18*), which suggested that phosphorylation of these proteins occurred on serine residues. SRP40 and NSR1 have very long stretches of serine residues that preclude precise mapping by site-directed mutagenesis. However, Nopp140, the mammalian homolog of SRP40 (*14*), has several short serine stretches surrounded by acidic amino acids. 5β[^{32}P]IP_7 phosphorylated both Nopp140 and Treacher Collins–Franceschetti syndrome 1 (TCOF1) protein, another mammalian nucleolar protein having short acidic serine stretches (*20*, *21*) (fig. S5).

Phosphorylation of regions consisting of amino acids 1 to 241, 1 to 100, and 1 to 75 of

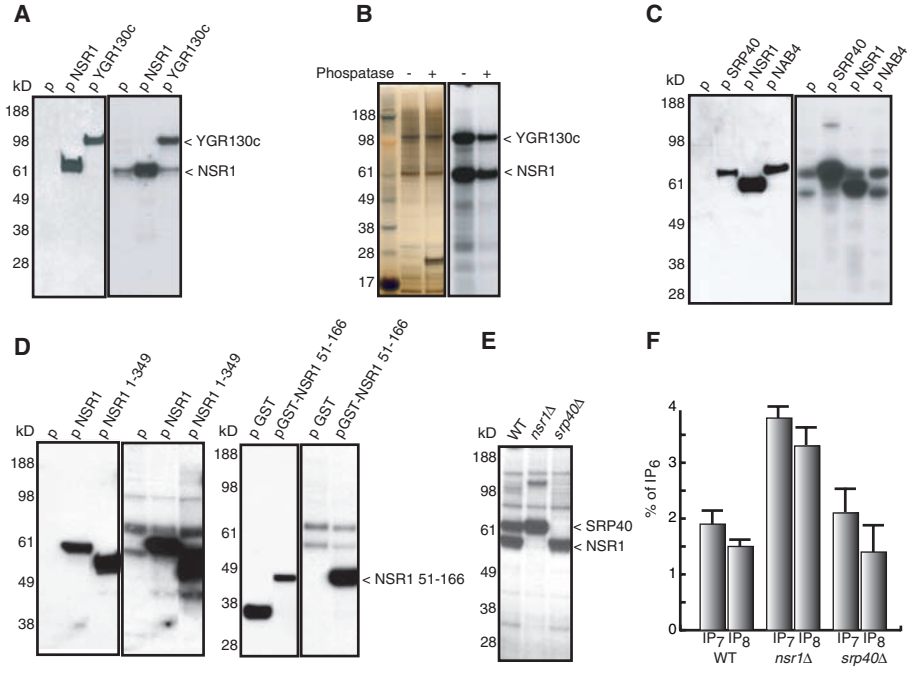

Fig. 2. Identification of 5β[^{32}P]IP_7 phosphorylation targets. (**A**) IP_7 phosphorylates NSR1 and YGR130c. Crude extracts from yeast overexpressing NSR1 or YGR130c (20 μg) were incubated with 0.5 μCi of 600 Ci/mmol 5β[^{32}P]IP_7 for 30 min at 37°C, followed by incubation at 95°C for 5 min in the presence of sample buffer. Samples were then separated by NuPAGE and transferred onto a nitrocellulose membrane. An autoradiogram of the membrane was obtained in order to visualize radiolabeled proteins (right) and subsequently analyzed by Western blot for Xpress tag (left) to assess protein expression. (**B**) Lambda phosphatase diminishes NSR1 and YGR130c phosphorylation. Purified NSR1 and YGR130c were incubated with 5β[^{32}P]IP_7 as described (*26*), in the presence (+) or absence (–) of lambda phosphatase (40 U). The gel was subjected to silver staining (left) and autoradiography (right). (**C** and **D**) Identifying consensus sequences for IP_7 phosphorylation. Extracts from yeast expressing full-length NSR1, NAB4, and SRP40 (C), or NSR1 fragments fused to an Xpress tag or to GST (D) were incubated with 5β[^{32}P]IP_7 and processed as described in (A). (**E**) SRP40 is a target of IP_7 phosphorylation. Protein extracts of wild-type, *nsr1*Δ, and *srp40*Δ yeast were incubated with 5β[^{32}P]IP_7 and processed as described in (A). (**F**) Inositol pyrophosphate levels are augmented by deletion of *nsr1*. Analysis of the intracellular concentration of inositol pyrophosphates in wild-type, *nsr1*Δ, and *srp40*Δ yeast. The concentrations of the inositol pyrophosphates IP_7 and IP_8 are expressed as a percentage of their ratio to IP_6 concentration. Data represent the means and SEM of three independent determinations. Concentrations of inositol phosphates were determined as described (*26*).

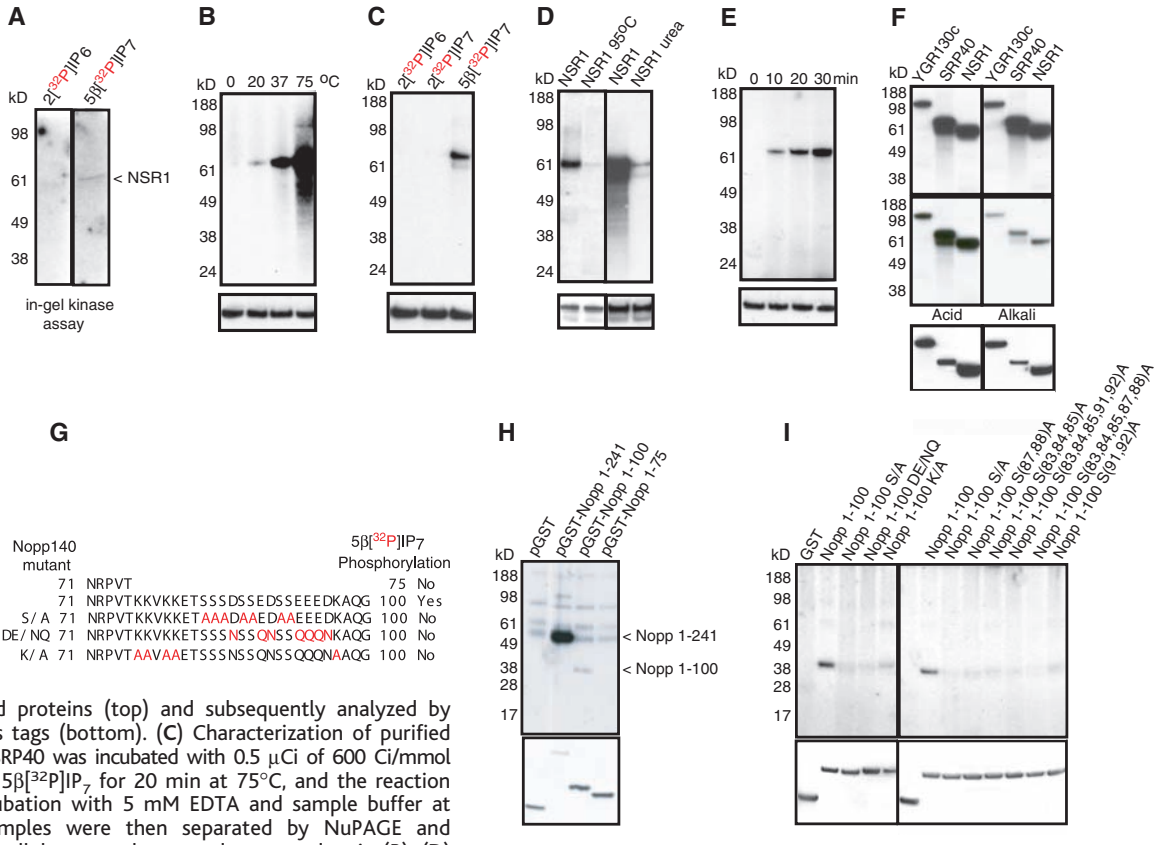

Fig. 3. Characterization of 5β[^{32}P]IP$_7$ phosphorylation. (**A**) 5β[^{32}P]IP$_7$ -driven protein phosphorylation does not require kinases. Autoradiograms of purified NSR1 subjected to denaturing SDS-PAGE and in-gel kinase assay (*26*). (**B**) Temperature-dependent phosphorylation of purified SRP40. SRP40 was incubated with 5β[^{32}P]IP$_7$ for 10 min. Phosphorylation assays were performed at the indicated temperatures, and sample buffer was added at room temperature. Samples were then separated by NuPAGE and transferred onto a nitrocellulose membrane. An autoradiogram of the membrane was obtained in order to visualize radiolabeled proteins (top) and subsequently analyzed by Western blot for Xpress tags (bottom). (**C**) Characterization of purified SRP40 phosphorylation. SRP40 was incubated with 0.5 μCi of 600 Ci/mmol 2[^{32}P]IP$_6$, 2[^{32}P]IP$_7$, and 5β[^{32}P]IP$_7$ for 20 min at 75°C, and the reaction was terminated by incubation with 5 mM EDTA and sample buffer at room temperature. Samples were then separated by NuPAGE and transferred onto a nitrocellulose membrane and processed as in (B). (**D**) Denatured NSR1 is not phosphorylated by 5β[^{32}P]IP$_7$. Purified, native NSR1 (at room temperature), heat-denatured NSR1 (at 95°C), or chemically denatured NSR1 (in 6 M urea), were incubated for 10 min with 5β[^{32}P]IP$_7$. Reactions were then incubated for 5 min at 95°C, separated by NuPAGE, and processed as in (B). (**E**) Time course of IP$_7$ phosphorylation of purified SRP40. SRP40 was incubated with 0.5 μCi of 600 Ci/mmol of 5β[^{32}P]IP$_7$ at 37°C for the indicated length of time. The reactions were terminated by adding 5 mM EDTA and sample buffer at room temperature; the samples were separated by NuPAGE and processed as in (B). (**F**) Alkali sensitivity of 5β[^{32}P]IP$_7$ phosphorylated proteins. YGR130c, SRP40, and NSR1 (20 to 50 ng) phosphorylated by 5β[^{32}P]IP$_7$ were separated by NuPAGE and transferred onto a PVDF membrane. An autoradiogram of the membrane was obtained in order to visualize radiolabeled proteins (top). Subsequently the membranes were subject to alkali or acid treatment (*26*), followed by a second autoradiogram (center). Xpress-tag Western blotting (bottom) was then performed to assess protein presence. (**G**) Amino acid sequences of the regions between residues 70 and 100 of mouse Nopp140 phosphorylated by 5β[^{32}P]IP$_7$. Mutations are highlighted in red, and the results of in vitro phosphorylation of these mutants by 5β[^{32}P]IP$_7$ are indicated. (**H**) Identification of IP$_7$ phosphorylation domain in Nopp140. Crude extracts (20 μg) from yeast overexpressing mouse Nopp140 fragments fused to GST were incubated with 0.5 μCi of 600 Ci/mmol 5β[^{32}P]IP$_7$ for 20 min at 37°C, followed by incubation at 95°C for 5 min in the presence of sample buffer. Samples were then separated by NuPAGE and transferred onto a nitrocellulose membrane. An autoradiogram of the membrane was obtained in order to visualize radiolabeled proteins (top) and subsequently subjected to GST antibody tag Western blotting (bottom) to assess protein expression. (**I**) Identification of the residues required for IP$_7$ phosphorylation. Purified Nopp140 fragments (1 μg) expressed as GST fusion proteins were incubated with 1 μCi of 60 Ci/mmol 5β[^{32}P]IP$_7$ for 15 min at 37°C and then in sample buffer at 95°C for 5 min. The proteins were separated by NuPAGE polyacrylamide gel electrophoresis (Novex), stained by Coomassie brilliant blue R-250 (bottom), and subject to autoradiography (top).

Nopp140 was assessed in the context of glutathione *S*-transferase (GST) fusion proteins (Fig. 3H). The most robust phosphorylation occurred with region 1 to 241, less with 1 to 100, and none was detected in region 1 to 75, which indicated that the seven Ser residues in Nopp140 between amino acids 75 and 100 are possible targets of phosphorylation (Fig. 3, G and H). Mutagenesis of these Ser residues to Ala abrogated phosphorylation by 5β[^{32}P]IP$_7$ (Fig. 3I). Because phosphorylation of the 1– to 241–amino acid fragment was greater than the 1– to 100–amino acid fragment, we assume that other acidic Ser residues within the 127 to 136 and 170 to 179 amino acid sequences are also potential phosphorylation targets. To map the exact phosphorylated Ser residues, we made combinatorial substitutions of two or more Ser with Ala within the 1– to 100–amino acid region of Nopp140 (Fig. 3I). Each mutant showed a decrease in phosphorylation, suggesting that multiple serines are phosphorylated, although it is conceivable that multiple serine mutations affect phosphorylation by altering the protein's secondary structure. The acidic amino acids that flank the serine stretches are critical, as their mutation resulted in loss of phosphorylation (Fig. 3I). The regions of phosphorylation by IP$_7$ also contain multiple lysines, the mutation of which dramatically decreased phosphorylation (Fig. 3I). The acidic amino acids are presumably required for binding to magnesium, whereas the lysine residues may coordinate the phosphate groups of IP$_7$. The failure of lysine mutations to abolish phosphorylation indicates that the lysines may not be absolutely critical.

To establish that IP$_7$ phosphorylation occurs with endogenous IP$_7$ and endogenous substrate proteins in intact cells, we focused on NSR1. NSR1 phosphorylation in vitro increased in extracts from yeast lacking IP6K (also know as KCS1, ORF YDR017c), which suggested that a major portion of endogenous NSR1 is phosphorylated under basal conditions by IP$_7$ (fig. S6). Endogenous IP$_7$ was radiolabeled by incubating yeast with [^{32}PO$_4$]$_i$ orthophosphate. Because IP6K plays a role in phosphate uptake (*22*, *23*), phosphate accumulation was reduced in yeast lacking IP6K (*ip6kΔ*) (fig. S7). To overcome the difficulties associated with overexpression, we used TAP (tandem affinity purification) yeast strains (*15*)

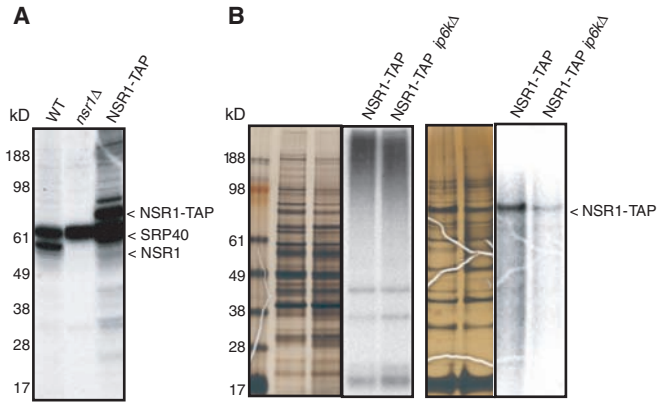

Fig. 4. In vivo 5β[^{32}P]IP$_7$ phosphorylation. (**A**) Presence of an 80-kD phosphorylated band in the NSR1-TAP strain. Wild-type, *nsr1*Δ, and wild-type NSR1-TAP yeast extracts were incubated with 5β[^{32}P]IP$_7$ and processed as described in Fig. 2. (**B** and **C**) IP6K deletion reduces phosphorylation of NSR1 by endogenous IP$_7$. (B) Wild-type NSR1-TAP and NSR1-TAP *ip6k*Δ yeast were labeled with [^{32}PO$_4$]$_i$ orthophosphate, and TAP-NSR1 was purified as described (*26*). Yeast homogenates (2 μg) were subjected to NuPAGE, and the gel was silver stained and autoradiographed to demonstrate equal levels of basal phosphorylation (left). Silver staining and autoradiogram of purified NSR1-TAP from wild-type and *ip6k*Δ yeast (right). (C) Quantification of the relative phosphorylation of NSR1-TAP purified from wild-type or *ip6k*Δ yeast. Data represent the mean values and SEM from three independent experiments.

to purify endogenous [^{32}PO$_4$]-labeled NSR1-TAP from both wild-type NSR1-TAP and *ip6k*Δ NSR1-TAP yeast (Fig. 4A). Lack of IP6K resulted in an almost 60% decline in phosphorylation of NSR1 in vivo, indicating that this protein is physiologically phosphorylated in intact cells by endogenous IP$_7$ (Fig. 4, B and C).

This study establishes that the inositol pyrophosphate IP$_7$ is a physiologic phosphate donor to a range of proteins in eukaryotic cells. The proteins we have best characterized as IP$_7$ targets, yeast NSR1 and SRP40 and mammalian Nopp140 and TCOF1, are nucleolar proteins involved in ribosomal biogenesis. Additionally, IP$_7$ phosphorylation of proteins involved in endocytosis may mediate roles of inositol pyrophosphates in this process (*6*), consistent with the phosphorylation by IP$_7$ of the adaptin β3A subunit (*18*), a regulator of vesicular trafficking (*24*, *25*).

References and Notes

1. L. Stephens *et al.*, *J. Biol. Chem.* **268**, 4009 (1993).
2. F. S. Menniti, R. N. Miller, J. W. Putney Jr., S. B. Shears, *J. Biol. Chem.* **268**, 3850 (1993).
3. R. F. Irvine, M. J. Schell, *Nat. Rev. Mol. Cell Biol.* **2**, 327 (2001).
4. A. Saiardi, H. Erdjument-Bromage, A. M. Snowman, P. Tempst, S. H. Snyder, *Curr. Biol.* **9**, 1323 (1999).
5. A. Saiardi, E. Nagata, H. R. Luo, A. M. Snowman, S. H. Snyder, *J. Biol. Chem.* **276**, 39179 (2001).
6. A. Saiardi, C. Sciambi, J. M. McCaffery, B. Wendland, S. H. Snyder, *Proc. Natl. Acad. Sci. U.S.A.* **99**, 14206 (2002).
7. H. R. Luo *et al.*, *Cell* **114**, 559 (2003).
8. B. H. Morrison, J. A. Bauer, D. V. Kalvakolanu, D. J. Lindner, *J. Biol. Chem.* **276**, 24965 (2001).
9. T. Laussmann, R. Eujen, C. M. Weisshuhn, U. Thiel, G. Vogel, *Biochem. J.* **315**, 715 (1996).
10. S. M. Voglmaier *et al.*, *Proc. Natl. Acad. Sci. U.S.A.* **93**, 4305 (1996).
11. Z. Xue, T. Melese, *Trends Cell Biol.* **4**, 414 (1994).
12. T. Stage-Zimmermann, U. Schmidt, P. A. Silver, *Mol. Biol. Cell* **11**, 3777 (2000).
13. S. M. Wilson, K. V. Datar, M. R. Paddy, J. R. Swedlow, M. S. Swanson, *J. Cell Biol.* **127**, 1173 (1994).
14. U. T. Meier, *J. Biol. Chem.* **271**, 19376 (1996).
15. S. Ghaemmaghami *et al.*, *Nature* **425**, 737 (2003).
16. S. T. Safrany *et al.*, *J. Biol. Chem.* **274**, 21735 (1999).
17. E. A. Winzeler *et al.*, *Science* **285**, 901 (1999).
18. A. Saiardi, R. Bhandari, S. H. Snyder, unpublished observation.
19. B. Duclos, S. Marcandier, A. J. Cozzone, *Methods Enzymol.* **201**, 10 (1991).
20. Treacher Collins Syndrome Collaborative Group, *Nature Genet.* **12**, 130 (1996).
21. W. A. Paznekas, N. Zhang, T. Gridley, E. W. Jabs, *Biochem. Biophys. Res. Commun.* **238**, 1 (1997).
22. F. Norbis *et al.*, *J. Membr. Biol.* **156**, 19 (1997).
23. M. J. Schell *et al.*, *FEBS Lett.* **461**, 169 (1999).
24. E. C. Dell'Angelica, C. E. Ooi, J. S. Bonifacino, *J. Biol. Chem.* **272**, 15078 (1997).
25. E. C. Dell'Angelica, V. Shotelersuk, R. C. Aguilar, W. A. Gahl, J. S. Bonifacino, *Mol. Cell* **3**, 11 (1999).
26. Materials and methods are available as supporting material on *Science* online.

27. We thank A. Riccio, B. Wendland, H. R. Luo, and T. R. Raghunand for suggestions, discussions, and helpful comments and all the members of the Snyder lab for creating a stimulating environment. This work was supported by U.S. Public Health Service Grant MH18501, Conte Center Grant MH068830-02, and Research Scientist Award DA00074 (to S.H.S.).

Supporting Online Material
www.sciencemag.org/cgi/content/full/306/5704/2101/DC1
Materials and Methods
Figs. S1 to S7
References and Notes

28 July 2004; accepted 29 October 2004
10.1126/science.1103344

Nutrient Availability Regulates SIRT1 Through a Forkhead-Dependent Pathway

Shino Nemoto, Maria M. Fergusson, Toren Finkel*

Nutrient availability regulates life-span in a wide range of organisms. We demonstrate that in mammalian cells, acute nutrient withdrawal simultaneously augments expression of the SIRT1 deacetylase and activates the Forkhead transcription factor Foxo3a. Knockdown of Foxo3a expression inhibited the starvation-induced increase in SIRT1 expression. Stimulation of SIRT1 transcription by Foxo3a was mediated through two p53 binding sites present in the SIRT1 promoter, and a nutrient-sensitive physical interaction was observed between Foxo3a and p53. SIRT1 expression was not induced in starved p53-deficient mice. Thus, in mammalian cells, p53, Foxo3a, and SIRT1, three proteins separately implicated in aging, constitute a nutrient-sensing pathway.

In the yeast *Saccharomyces cerevisiae* and in the nematode *Caenorhabditis elegans*, life-span can be extended by increasing the expression of the deacetylase Sir2, an enzyme whose activity depends on the oxidized form of nicotinamide adenine dinucleotide (NAD) (*1*, *2*). In these model organisms, the ability of Sir2 to extend life may be related to its role in gene silencing. In both the nematode and yeast, certain simple environmental stresses can also increase life-span. In yeast, reducing the amount of available glucose has this effect. The ability of glucose restriction to increase the life-span of yeast requires Sir2 (*3*). In *C. elegans*, activation of the Forkhead transcription factor DAF-16 is also associated with increased life-span (*4*) and its activation depends in part on nutrient availability (*5*). Genetic evidence further suggests that in worms, DAF-16 and Sir2 work through a common pathway (*2*), and recent evidence suggests that their mammalian counterparts physically interact (*6*, *7*).

Here, we further analyzed the interrelationship of the closest mammalian orthologs

Cardiovascular Branch, National Heart, Lung, and Blood Institute (NHLBI), Bethesda, MD 20892, USA.

*To whom correspondence should be addressed. E-mail: finkelt@nih.gov